ChemComm

COMMUNICATION

View Article Online
View Journal | View Issue

Check for updates

Cite this: *Chem. Commun.*, 2024, **60**, 11335

Received 13th July 2024,
Accepted 13th September 2024

DOI: 10.1039/d4cc03491k

rsc.li/chemcomm

Published on 13 September 2024. Downloaded on 5/9/2026 1:08:15 PM.

A multifunctional phenylphosphinamide additive for stable flexible inverted perovskite solar cells†

Feihu Liu, Jidong Geng, Wei Zhang, Jie Dou, * Qiyao Guo, Jialong Duan and Qunwei Tang *

The multifunctional phenylphosphinamide additive is used in flexible inverted perovskite solar cells to release tensile strain and increase the toughness of the perovskite film, achieving enhanced device efficiency and stability.

Organic–inorganic hybrid metal halide perovskite materials have the advantages of high carrier mobility, wide spectral response range, long diffusion distance, and large absorption coefficient, and the related solar cell exhibited excellent photovoltaic performance.[1,2] Since 2009, the certified photovoltaic conversion efficiency (PCE) of these perovskite solar cells (PSCs) has increased from 3.8% to 26.7% in just over a decade.[3] In addition, the perovskite film is applied in the field of flexible devices due to its high anisotropy, low shear modulus, and mechanical hardness. Therefore, these flexible perovskite solar cells (f-PSCs) have the characteristics of light weight, high toughness, and easy deformation.[4,5] Stability, especially mechanical stability, is one of the critical issues for determining the industrialization of f-PSCs.[6]

Significant endeavors have been undertaken to enhance the mechanical characteristics of f-PSCs. To improve crystal packing at the buried interface and reduce lattice strain throughout the flexible perovskite film, the organic bifunctional passivator sodium 2-cyanoacetate,[7] histamine diiodate,[8] Y6,[9] $HCOONH_4$,[10] borax,[11] random copolymerization of acrylamide and *n*-butyl acrylate,[12] and other molecules are employed at the perovskite interface. In addition, Yuanyuan Zhou's group[13] devised an interpenetrating interface between the perovskite and electron-transporting layer to minimize the propensity for interfacial fracture. By adjusting the substrate thickness and employing the neutral plane concept, Mansoo Choi *et al.*[14] obtained crack-free polycrystalline perovskite films. However, the interface treatment has almost no effect on the mechanical properties of perovskite. The stability of flexible devices relies on the mechanical properties of the active layer. For the active layer, bulk phase doping by ionic liquids[15,16] or low-dimensional perovskite[17,18] doping can also improve the mechanical endurance of f-PSCs. Small-molecule additives could also improve the mechanical properties of perovskite active layers (such as elastic modulus, coefficient of thermal expansion, ductility, *etc.*). Nevertheless, whether it is an ionic liquid or a low-dimensional perovskite, the preparation process is complicated. Therefore, there is an urgent need to develop simple molecules to enhance the mechanical reliability of f-PSCs.

In this study, the dual-passivation additive phenylphosphinamide (DPPA) is added into the perovskite film and used to fabricate f-PSCs. The interaction between the DPPA and perovskite has an important impact on the mechanical and physicochemical properties of the active layer. Due to the released strain and suitable energy level structure, the f-PSC with DPPA achieved an efficiency of 20.46%. Moreover, the operational lifespan of the device was prolonged owing to low ion migration and high elasticity of the perovskite film.

According to the interaction mechanism, the chemical structure of the organic molecule DPPA contains a phosphine oxide group and an amino group (Fig. S1, ESI†). Density functional theory (DFT) calculation was utilized to investigate the charge distribution, dipole moment, and electronegativity of DPPA. The –P═O group predominantly bears the overall negative charge of the molecule, while the -NH_2 group primarily harbors positive charge. Considering the Lewis base-acid theory, we speculate that the coordination of DPPA and perovskite occurs between the –P═O group and the exposed Pb^{2+} ions. The –NH_2 group will likely interact with the adjacent halide ions through weak electrostatic or hydrogen-bonding interactions. To verify the above speculation, we carried out measurements using Fourier transform infrared spectroscopy (FTIR) and X-ray photoelectron spectroscopy (XPS) in Fig. 1. As shown in Fig. 1c, the stretching vibration peak corresponding to the –P═O group within DPPA is located at 1173 cm^{-1}, whereas the

Institute of Carton Neutrality, College of Chemical and Biological Engineering, Shandong University of Science and Technology, Qingdao 266590, P. R. China. E-mail: doujie@sdust.edu.cn, tangqunwei@sdust.edu.cn

† Electronic supplementary information (ESI) available. See DOI: https://doi.org/10.1039/d4cc03491k

Published on 13 September 2024. Downloaded on 5/9/2026 1:08:15 PM.

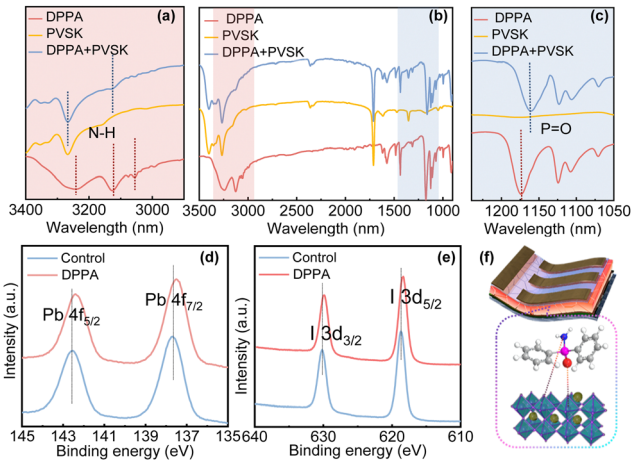

Fig. 1 (a)–(c) FTIR spectra of pure DPPA, perovskite, and DPPA-doped perovskite films; XPS spectra of perovskite and DPPA-doped perovskite films of (d) Pb 4f and (e) I 3d; (f) schematic illustration of the interaction between DPPA and perovskite.

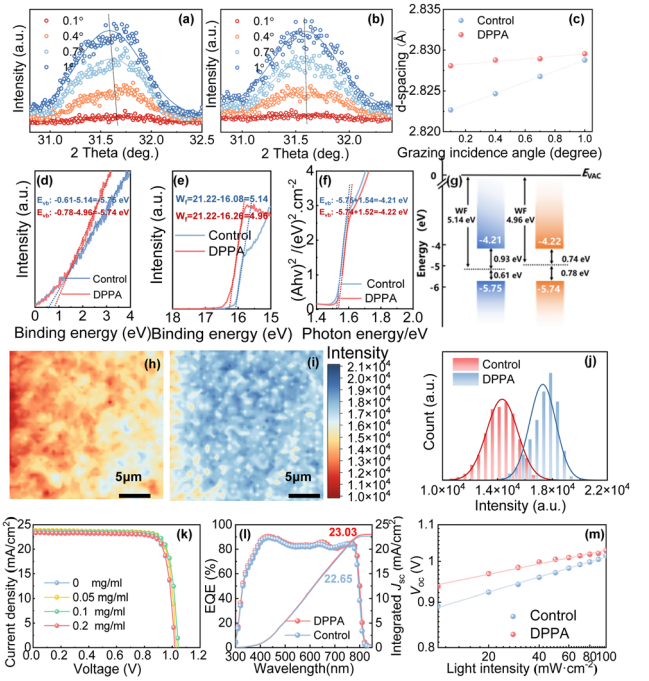

Fig. 2 GIXRD patterns of the perovskite films (a) without and (b) with DPPA; (c) *d*-spacing values as a function of the incidence angle; UPS spectra of the (d) Fermi edge and (e) cut-off energy of perovskite films, (f) the plots of $(Ah\nu)^2$ *versus* photon energy ($h\nu$) of the perovskite films, (g) the schematic band alignment of between perovskite; PL mapping maps of the perovskite films (h) without and (i) with DPPA, (j) the related PL intensity distribution chart; (k) *J*–*V* curves of the champion f-PSCs with different DPPA concentrations; (l) EQE spectra; (m) the plots of V_{OC} upon light intensity.

stretching vibration peak of the DPPA-doped perovskite is situated at 1161 cm^{-1}. The shift of this peak in the FTIR spectrums confirms the coordination between the –P═O group and the perovskite. Fig. 1a depicts distinct vibrational modes in the amino group, including asymmetric N–H stretching at 3243 cm^{-1}, symmetric N–H stretching at 3122 cm^{-1}, and an overtone of N–H bending at 3055 cm^{-1}. However, notable shifts in the amino group peaks are observed in the perovskite containing DPPA, suggesting the formation of hydrogen bonds between the amino group and the halide ions of the perovskite. The introduction of DPPA into the pure perovskite film led to a noticeable shift in the Pb 4f peaks from 142.6 eV and 137.7 eV to 142.3 eV and 137.4 eV, respectively (Fig. 1d). This suggests potential for the formation of a coordinate bond between the Pb^{2+} ion and the oxygen atom in the P═O group, wherein the oxygen atom donates its lone pair electrons to the empty orbital of the Pb^{2+} ion. Compared to pure perovskite, the XPS peaks of I 3d of DPPA-doped perovskite are shifted toward lower binding energies, which verified that the I element had formed a connection with the –N–H group (Fig. 1e). The reduction in the binding energy of I^- can be attributed to the assisting role of hydrogen bonding. The related interaction mechanism is illustrated in Fig. 1f. Furthermore, the incorporation of DPPA into the perovskite enhances its crystallinity and minimizes grain boundaries, which is crucial for enhancing the overall quality of the perovskite film in Fig. S2 and S3 (ESI†).

To explore the effect of interaction on the mechanical properties of perovskite film, grazing incident X-ray diffraction (GIXRD) is performed in Fig. 2a–c. When varying the grazing incident angles from 0.1 to 1, the characteristic peak shifts to lower angles. According to Bragg's Law, this shift indicated an increasing spacing between the crystal planes perpendicular to the hole transport layer. The difference in material during the cooling process resulted in a mismatch in lattice dimensions, creating strain within the material.[19] There is a significantly reduced diffraction peak shift by introducing the DPPA. This means that the reduction in crystal lattice contraction decreases the tensile stress and reduces the strain-induced lattice distortion. As a result, the additive of DPPA enhances the robustness against considerable mechanical stress of the perovskite films. Based on the modified electronic structure within the strained perovskite, we try to elucidate the impact of residual strains on the mechanism of charge carrier transport in perovskite solar cells. Fig. 2d–g display the evolution of the band-edge energies. The conduction band minimum (CBM) and valence band maximum (VBM) of the DPPA-doped perovskite film are nearly identical to the pure perovskite film. The work function (W_F) undergoes a shift of approximately 180 meV towards the vacuum level (E_{VAC}), while the Fermi level (E_F) shifts by 390 meV in the direction of the CBM. This indicated that the DPPA-doped perovskite films become more n-type, which is favorable for the charge transfer between the perovskite itself and the electron transport material.[20] To evaluate the impact of strain on charge-carrier transport behavior, we also conducted photoluminescence (PL) mapping (Fig. 2h–j), steady-state PL (Fig. S4a, ESI†), and time-resolved PL (TRPL, Fig. S4b, ESI†) measurements for both control and DPPA-doped perovskite films on glass substrates. The PL intensity mapping of the DPPA-doped perovskite film reveals a significantly stronger and more uniform distribution than the control film. In addition, the enhanced intensity of PL and related PL mapping indicates

 This journal is © The Royal Society of Chemistry 2024

Published on 13 September 2024. Downloaded on 5/9/2026 1:08:15 PM.

a reduction in carrier recombination, suggesting improved charge transport properties. Notably, the TRPL results demonstrate an increase in carrier lifetime, rising from 571 ns in the control film to 909 ns in the DPPA-doped one. This significant enhancement in carrier lifetime further supports the reduced recombination and improved charge transport in the DPPA-doped perovskite film.

To further investigate the effect of the strain on the photovoltaic properties, we fabricated the f-PSCs without and with DPPA by the current–density voltage (J–V) characteristics of the champion devices (Fig. 2k and Table S1, ESI†). Compared to the control device, the open-circuit voltage (V_{oc}) of the PSC with 0.1 mg mL^{-1} DPPA has significantly improved. The DPPA-doped device exhibited a short-circuit current density (J_{sc}) of 23.63 mA cm^{-2}, an open-circuit voltage (V_{oc}) of 1.043 V, an FF of 82.97%, and an efficiency of 20.46%. To avoid possible misleading with sample variation, we fabricated 15 cells without and with DPPA, respectively. These box plots of two kinds of cells further verified the PCE enhancement in Fig. S5 (ESI†). The DPPA-doped devices obtained an average PCE of 19.1%, higher than the control devices (18.2%). In addition, after the doping treatment, the device exhibited reduced hysteresis (Fig. S6a and Table S2, ESI†). The external quantum efficiency (EQE) spectra are displayed in Fig. 2l. Compared to the control device, the DPPA-doped device showed a higher light harvesting efficiency (EQE value is close to 90%) along the UV-vis absorption wavelength range from 300 to 850 nm. Fig. 2m depicts plots of V_{oc} with increasing light intensity after doping, showing a decrease in slope from 1.984 to 1.405k_B T q^{-1}. The ideality factor decrease shows that incorporating DPPA into the device reduces charge carrier recombination, resulting in an improved V_{oc} value. These plots of J_{sc} upon light intensity exhibit a similar trend as the V_{oc} curve (Fig. S6b, ESI†). The closer the value of the ideality factor is to 1, the less carrier recombination channels. We further conducted electrical impedance spectroscopy (EIS) testing to assess the contact resistance (R_{co}) and recombination resistance (R_{rec}) in Fig. S6c (ESI†). The results revealed an increased R_{rec}, from 9.13 to 11.23 KΩ, for the devices with DPPA. This decreased value of R_s and increased value of R_{rec} suggest a significant improvement in charge transportation at the perovskite contact interface. Furthermore, the increased built-in potential (V_{bi}) obtained from the Mott–Schottky (M–S) curves (see Fig. S6d, ESI†) indicates a stronger driving force, resulting in a significantly lower dark current density for the leading device. In turn, this results in the enhancement of V_{oc}, indicating improved performance in the photovoltaic device.

To evaluate the stability of the devices, the maximum power point (MPP) was tracked in a nitrogen atmosphere and the normalized PCE was monitored continuously under LED lamp irradiation and J–V testing in an air environment with humidity (10–40%) and temperature (10–20 °C) in Fig. 3a and b. The flexible devices with DPPA maintained 80% of their original PCE for over 900 h, whereas the control cells kept 80% of their original PCE for less than 400 h. In short, it demonstrated that the integration of DPPA significantly enhanced the light

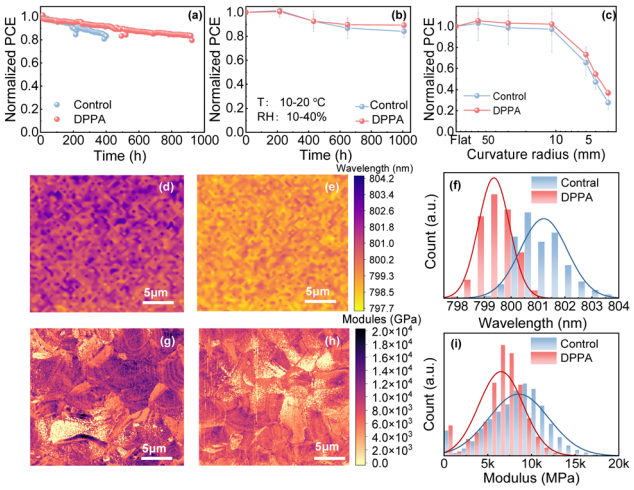

Fig. 3 (a) MPP tracking of the device at 0.89 V; these f-PSCs as a function of (b) the storage time in an air environment and (c) bending radii under bending for 1 cycle; PL mapping maps of perovskite films (d) without and (e) with DPPA, and (f) the related peak wavelength distribution chart; elastic modulus maps of the perovskite films (g) without and (h) with DPPA, and (i) the related Young's modulus distribution.

stability of the flexible devices. As shown in Fig. 3b and Fig. S7a–c (ESI†), after 1008 hours, the DPPA-doped f-PSCs retained only 89% of their original efficiency, whereas the control devices still maintained 84% of their initial efficiency. Therefore, DPPA treatment improves the humidity stability of the f-PSCs. It is widely recognized that the degradation of perovskite-based devices is mainly caused by two key factors: decomposition and phase transformation. Formamidinium cations in perovskites are particularly prone to phase transformation. Either light or water significantly threatens the stability of perovskite devices, speeding up ion migration within their inherent defects. This ion migration disrupts the charge transport, ultimately resulting in a decline in device performance and subsequent degradation.

The phase separation of perovskite films was further investigated through photoluminescence (PL) mapping in Fig. 3d–f. Compared to the control film, the blue shift observed in the PL peak of the DPPA-doped perovskite film is attributed to the formation of nonradiative recombination centers during oxidation. The DPPA-doped perovskite film exhibited a narrower wavelength range compared to the control film, which had a broader range and higher heterogeneity. This finding suggests that the chemical interactions induced by DPPA doping stabilize the perovskite crystals, effectively suppressing phase segregation and enhancing the overall homogeneity of the film.[21] The addition of DPPA might prevent phase separation by suppressing ion migration and volatile component escape, thus improving the light and humidity stability of flexible devices.

For flexible devices, mechanical reliability is a characteristic feature, and a cyclic bending test is used to evaluate mechanical durability. Under varying radii of curvature, the efficiency is recorded in Fig. 3c and Fig. S8a–c (ESI†). The control cell exhibits an obvious decline in FF under the bending condition of 12 mm, which may be due to the cracking of the perovskite

Published on 13 September 2024. Downloaded on 5/9/2026 1:08:15 PM.

layer. The DPPA-doped device retained 73% of the initial PCE after being bent to a radius of 5 mm. In contrast, the control devices retained merely 65% of their original PCE. These results indicate that DPPA plays a pivotal role in improving the mechanical stability of f-PSCs. As depicted in Fig. S9 (ESI†), control devices rapidly lose the value of PCE, exceeding 20% loss from their original value after 100 cycles of bending at a 10 mm radius. In contrast, the DPPA-modified PSCs exhibit superior longevity, retaining 83% of their original PCE. This decline in PCE is primarily attributed to the reduction in FF, which stems from the cracking of the perovskite film. To explore the factors contributing to the enhanced mechanical properties, we carried out a non-destructive peak force quantitative nano-mechanical mapping test. This approach obtained the surface-averaged elastic modulus data, which closely correlates with the flexibility of the perovskite. As illustrated in Fig. 3h and i, the DPPA-doped perovskite film exhibited an averaged elastic modulus of 7.25 GPa. This value is slightly lower than the reference films' modulus of 9.25 GPa. This implies that the perovskite film shows improved resistance to external forces such as mechanical stress, making it a favorable material for applications requiring durability and stability. These SEM images (Fig. S10, ESI†) reveal mechanical damage cracks in grains post-1 bending cycle with varying radii. These cracks may propagate, leading to severe crystal shedding upon further bending. Compared to reference one, DPPA-treated perovskite films show narrower, shallower cracks, enhancing resistance to cracking and mechanical stability. These cracks impede charge transport, increasing resistance, while DPPA modification mitigates cracking risks. As discussed above, the perovskite films released by DPPA have shown exceptional chemical and mechanical stability, contributing to the improved stability of the corresponding devices.

We introduce a novel strain evolution strategy involving the incorporation of DPPA into perovskite films to improve the stability of f-PSCs. DPPA is a versatile molecule with numerous interactive abilities, including the capacity to alleviate strain, fine-tune energy level structures, minimize ion migration, and enhance the elastic modulus of the perovskite film. As a result, high efficiency of 20.46% was achieved in f-PSCs, and unprecedented improvements in the operational stability, mechanical stability (T80 $>$ 900 h, MPP; T80 $>$ 1000 h, humidity), and humidity stability (T70 $>$ 5 mm) were also accomplished in f-PSCs. This approach paves the way for more reliable and durable solar energy solutions.

The authors gratefully acknowledged financial support provided by the National Natural Science Foundation of China (62304124, 62204098, 22109053, 62374105) and Special Fund of Taishan Scholar Program of Shandong Province (tsqnz20221141).

Data availability

The data supporting this article have been included as part of the ESI.†

Conflicts of interest

The authors declare no competing financial interests or personal relationships.

Notes and references

1 P. Chen, Y. Xiao, J. Hu, S. Li, D. Luo, R. Su, P. Caprioglio, P. Kaienburg, X. Jia, N. Chen, J. Wu, Y. Sui, P. Tang, H. Yan, T. Huang, M. Yu, Q. Li, L. Zhao, C.-H. Hou, Y.-W. You, J.-J. Shyue, D. Wang, X. Li, Q. Zhao, Q. Gong, Z.-H. Lu, H. J. Snaith and R. Zhu, *Nature*, 2024, **625**, 516–522.
2 Y. Zheng, C. Tian, X. Wu, A. Sun, R. Zhuang, C. Tang, Y. Liu, Z. Li, B. Ouyang, J. Du, Z. Li, X. Wu, J. Chen, J. Cai and C.-C. Chen, *Adv. Energy Mater.*, 2024, **36**, 2304486.
3 **https://www.nrel.gov/pv/cell-efficiency.html**.
4 J. Zhao, Z. Xu, Z. Zhou, S. Xi, Y. Xia, Q. Zhang, L. Huang, L. Mei, Y. Jiang, J. Gao, Z. Zeng and C. Tan, *ACS Nano*, 2021, **15**, 10597–10608.
5 J. Zhang, W. Zhang, H.-M. Cheng and S. R. P. Silva, *Mater. Today*, 2020, **39**, 66–88.
6 M. Lira-Cantú, *Nat. Energy*, 2017, **2**, 17115.
7 C. Liu, T. Yang, W. Cai, Y. Wang, X. Chen, S. Wang, W. Huang, Y. Du, N. Wu, Z. Wang, Y. Yang, J. Feng, T. Niu, Z. Ding and K. Zhao, *Adv. Mater.*, 2024, **35**, 2311562.
8 L. Yang, J. Feng, Z. Liu, Y. Duan, S. Zhan, S. Yang, K. He, Y. Li, Y. Zhou, N. Yuan, J. Ding and S. Liu, *Adv. Mater.*, 2022, **34**, 2201681.
9 H. Liu, Z. Zhang, Z. Su, W. Zuo, Y. Tang, F. Yang, X. Zhang, C. Qin, J. Yang, Z. Li and M. Li, *Adv. Sci.*, 2022, **9**, 2105739.
10 Z. Zheng, F. Li, J. Gong, Y. Ma, J. Gu, X. Liu, S. Chen and M. Liu, *Adv. Mater.*, 2022, **34**, 2109879.
11 C. H. Chen, Z. H. Su, Y. H. Lou, Y. J. Yu, K. L. Wang, G. L. Liu, Y. R. Shi, J. Chen, J. J. Cao, L. Zhang, X. Y. Gao and Z. K. Wang, *Adv. Mater.*, 2022, **34**, 2200320.
12 C. Ge, X. Liu, Z. Yang, H. Li, W. Niu, X. Liu and Q. Dong, *Angew. Chem., Int. Ed.*, 2022, **61**, 202116602.
13 Q. Dong, C. Zhu, M. Chen, C. Jiang, J. Guo, Y. Feng, Z. Dai, S. K. Yadavalli, M. Hu, X. Cao, Y. Li, Y. Huang, Z. Liu, Y. Shi, L. Wang, N. P. Padture and Y. Zhou, *Nat. Commun.*, 2021, **12**, 973.
14 G. Lee, M.-c Kim, Y. W. Choi, N. Ahn, J. Jang, J. Yoon, S. M. Kim, J.-G. Lee, D. Kang, H. S. Jung and M. Choi, *Energy Environ. Sci.*, 2019, **12**, 3182–3191.
15 D. Yang, R. Yang, K. Wang, C. Wu, X. Zhu, J. Feng, X. Ren, G. Fang, S. Priya and S. F. Liu, *Nat. Commun.*, 2018, **9**, 3239.
16 C. Bi, B. Chen, H. Wei, S. DeLuca and J. Huang, *Adv. Mater.*, 2017, **29**, 1605900.
17 Q. Dong, M. Chen, Y. Liu, F. T. Eickemeyer, W. Zhao, Z. Dai, Y. Yin, C. Jiang, J. Feng, S. Jin, S. Liu, S. M. Zakeeruddin, M. Grätzel, N. P. Padture and Y. Shi, *Joule*, 2021, **5**, 1–15.
18 L. Hu, Q. Zhao, S. Huang, J. Zheng, X. Guan, R. Patterson, J. Kim, L. Shi, C. H. Lin, Q. Lei, D. Chu, W. Tao, S. Cheong, R. D. Tilley, A. W. Y. Ho-Baillie, J. M. Luther, J. Yuan and T. Wu, *Nat. Commun.*, 2021, **12**, 466.
19 Q. Zhou, J. Duan, J. Du, Q. Guo, Q. Zhang, X. Yang, Y. Duan and Q. Tang, *Adv. Sci. Lett.*, 2021, **8**, 2198–3844.
20 C. Zhu, X. Niu, Y. Fu, N. Li, C. Hu, Y. Chen, X. He, G. Na, P. Liu, H. Zai, Y. Ge, Y. Lu, X. Ke, Y. Bai, S. Yang, P. Chen, Y. Li, M. Sui, L. Zhang, H. Zhou and Q. Chen, *Nat. Commun.*, 2019, **10**, 815–826.
21 C. Qiu, J. Song, Y. Wu, X. Yin, L. Hu, Z. Su, Y. Jin, W. Wang, H. Wang and Z. Li, *Chem. Commun.*, 2023, **59**, 6414.

 This journal is © The Royal Society of Chemistry 2024